STRUCTURAL BIOLOGY COMMUNICATIONS

ISSN 2053-230X

Malonate in the nucleotide-binding site traps human AKAP18γ/δ in a novel conformational state

Kaare Bjerregaard-Andersen,[a]‡ Ellen Østensen,[b] John D. Scott,[c] Kjetil Taskén[a,b] and Jens Preben Morth[a]*

[a]Centre for Molecular Medicine Norway, University of Oslo, PO Box 1137, N-0318 Oslo, Norway, [b]Biotechnology Centre, University of Oslo, PO Box 1137, N-0318 Oslo, Norway, and [c]Howard Hughes Medical Institute and Department of Pharmacology, University of Washington, PO Box 357370, Seattle, WA 98195, USA. *Correspondence e-mail: j.p.morth@ncmm.uio.no

Received 10 May 2016
Accepted 21 June 2016

Edited by T. C. Terwilliger, Los Alamos National Laboratory, USA

‡ Present address: Department of Chemistry, University of Oslo, Norway.

Keywords: A-kinase anchoring protein; AKAP7; PKA; phospholamban; signalling; AKAP; drug design; PKA; proton wire.

PDB reference: AKAP18γ/δ, 5jj2

Supporting information: this article has supporting information at journals.iucr.org/f

A-kinase anchoring proteins (AKAPs) are a family of proteins that provide spatiotemporal resolution of protein kinase A (PKA) phosphorylation. In the myocardium, PKA and AKAP18γ/δ are found in complex with sarcoendoplasmic reticulum Ca^{2+}-ATPase 2 (SERCA2) and phospholamban (PLB). This macromolecular complex provides a means by which anchored PKA can dynamically regulate cytoplasmic Ca^{2+} release and re-uptake. For this reason, AKAP18γ/δ presents an interesting drug target with therapeutic potential in cardiovascular disease. The crystal structure of the central domain of human AKAP18γ has been determined at the atomic resolution of 1.25 Å. This first structure of human AKAP18γ is trapped in a novel conformation by a malonate molecule bridging the important R-loop with the 2H phosphoesterase motif. Although the physiological substrate of AKAP18γ is currently unknown, a potential proton wire deep in the central binding crevice has been indentified, leading to bulk solvent below the R-loop. Malonate complexed with AKAP18γ at atomic resolution provides an excellent starting point for structure-guided drug design.

1. Introduction

A-kinase anchoring proteins (AKAPs) are a family of proteins that control the spatiotemporal organization of protein kinase A (PKA) in the cell (Beene & Scott, 2007; Taskén & Aandahl, 2004). This enzyme is the principal target for cyclic adenosine monophosphate (cAMP), which is synthesized by adenylyl cyclases in the plasma membrane. Accumulation of cAMP within subcellular microdomains mandates the need to sequester the kinase within these areas and hence control its intracellular location (Zaccolo & Pozzan, 2002). AKAPs fulfil this function through complex association with PKA and other proteins and by their ability to tether these macromolecular complexes to intracellular membranes, the cytoskeleton and organelles (Wong & Scott, 2004). Because of their central role in organizing cAMP-dependent signalling events, AKAPs are now recognized as fundamental elements of most second messenger-responsive signalling pathways. For example, in the myocardium AKAP18 sequesters PKA with its substrates sarcoplasmatic reticulum Ca^{2+}-ATPase 2 (SERCA2) and phospholamban (PLB) (Lygren *et al.*, 2007). This AKAP18–PKA–SERCA2–PLB signalosome is a key modulator of Ca^{2+} signalling in myocytes during excitation–contraction coupling and is therefore of therapeutic interest in cardiovascular diseases.

A defining feature of all AKAPs is the presence of an amphipathic helix that forms a complex with the docking/dimerization (D/D) domain of the regulatory subunit of PKA

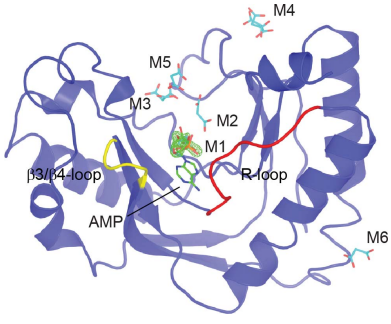

(Carr *et al.*, 1991). This molecular interface is responsible for irreversibly binding to the PKA holoenzymes. Selective targeting of AKAP signalling complexes to specific subcellular locations is mediated by protein–protein or protein–lipid interactions in other regions of the anchoring protein (Langeberg & Scott, 2015). Further diversity in AKAP assemblies is provided by the differential expression of alternately spliced forms. AKAP18 is found in four splice variants termed α, β, γ and δ. AKAP18γ and AKAP18δ are the longer variants and features a conserved central domain, AKAP18^{CD}, consisting of ∼200 amino acids. The complete AKAP18γ–PKA holoenzyme complex was recently determined by electron-microscopy single-particle reconstruction and shows that the AKAP18γ–D/D domain complex and the RIIα–PKAc complex domains are linked by large intrinsically disordered regions that retain intermolecular movement (Smith *et al.*, 2013).

The structure of the central domain of AKAP18δ from *Rattus norvegicus* has been determined in apo, AMP-bound and CMP-bound states (Gold *et al.*, 2008). These structures revealed a single-domain fold with a central cleft for the binding of AMP and CMP. Alignment with 2H phosphoesterase revealed a conserved fold and two His-*X*-Thr motifs required for phosphoesterase activity and suggest that the central domain may possess phosphoesterase activity. From sequence alignment, these have been shown to be conserved across species (Gold *et al.*, 2008). Here, we report the central domain of human AKAP18γ (hAKAP18γ^{CD}) trapped in the apo form by malonate at a resolution of 1.25 Å. The atomic resolution crystal structure is the first human representation of AKAP18. The R-loop and 2H phosphoesterase motif are bridged by a malonate molecule and thus are fixed. The high-resolution data allow us to confidently map a distinct water channel running in the bottom of the substrate-binding cleft, a water channel that may be modulated by the (V/A)G(E/D)SR(S/T) motif present in the R-loop.

2. Materials and methods

2.1. Macromolecule production

Primers for the ligation-independent cloning (LIC) of residues 71–288 encoding the central domain (CD) of human AKAP18γ (UniProt code Q9P0M2-1) into the pET-46 Ek/LIC vector (Novagen) were used. The construct was designed for the production of an N-terminally 6×His-tagged fusion protein termed hAKAP18γ^{CD}. A *Tobacco etch virus* (TEV) cleavage site was introduced for removal of the 6×His tag. The hAKAP18γ^{CD} construct was transformed into the *Escherichia coli* expression strain BL21-CodonPlus (Agilent Technologies). An overnight culture of 100 ml Luria–Bertani (LB) medium containing chloramphenicol (35 µg ml^{-1}) and ampicillin (50 µg ml^{-1}) was inoculated with a single colony of transformed *E. coli* BL21 cells. The overnight culture was diluted in 9 l LB medium with antibiotics as previously and 1 ml polyethylene glycol (an antifoam agent). The fermentation was left to grow until the optical density at 600 nm reached ∼1. The medium was chilled to 18°C and protein expression was induced with 1 m*M* IPTG. The cells were harvested after ∼18 h by centrifugation (9300*g*, 12 min), yielding ∼60 g wet weight of cells, which were stored at −80°C until use.

The cells were thawed on ice and 10 ml lysis buffer [500 m*M* NaCl, 100 m*M* Tris–HCl pH 8.0, 1 µg ml^{-1} DNAse I, 1 m*M* PMSF, 5 m*M* β-mercaptoethanol, 1× EDTA-free protease-inhibitor cocktail tablet (Roche), 40 m*M* imidazole] was added per gram of pellet. All chemicals were purchased from Sigma unless stated otherwise. The cells were lysed by forcing the suspension three times through a high-pressure homogenizer (Emulsiflex C3, Avestin). Cell debris was removed from the crude extract by centrifugation for 1 h at 200 000*g*. The cleared lysate was loaded onto a 5 ml Ni^{2+}-affinity column

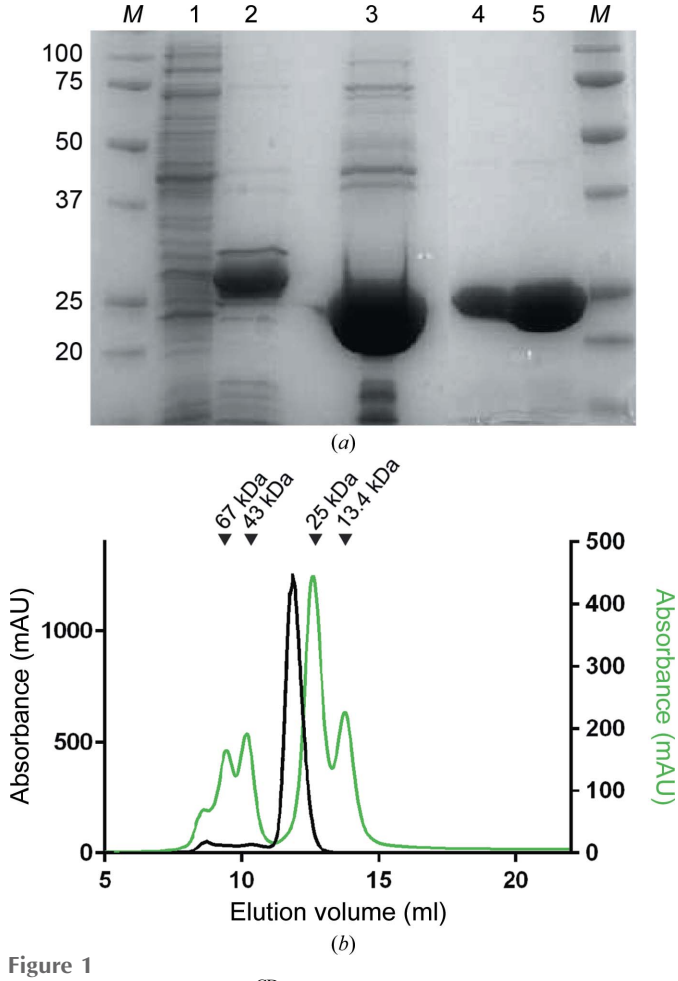

Figure 1
Purification of AKAP18γ^{CD}. (*a*) Coomassie Blue-stained 12% SDS–PAGE gel. Lane 1, clarified lysate. Lane 2, AKAP18γ^{CD} protein purified using Ni-Sepharose affinity chromatography. Lane 3, after cleavage of the His_6 tag with TEV protease. Lanes 4 and 5, purified AKAP18γ^{CD} separated by size-exclusion chromatography. Lanes labelled *M* contain molecular-weight markers (labelled in kDa). (*b*) Chromatogram representing the purification of AKAP18γ^{CD} (black) by size-exclusion chromatography using a Superdex 75 10/300 column. The retention volume compared with known standards indicates a monomer. The arrowheads indicate the peak elution positions of protein standards (green) with the given molecular weights: albumin (67 kDa), ovalbumin (43 kDa), chymotrypsinogen A (25 kDa) and ribonuclease A (13.7 kDa).

Table 1
Macromolecule-production information.

A TEV protease site was included in the forward primer and is underlined in the sequence. The cleavage site is denoted |.

Source organism	*Homo sapiens*
DNA source	Synthesized (GenScript)
Forward primer	GACGACGACAAGATGGAGAATCTTTATTTTCAGGGCGA-TCAAGTAAAGAAGAGGAAAAAA
Reverse primer	GAGGAGAAGCCCGGTTAGTTCTTTTCACCAATCACAAT-GG
Expression vector	pET-46 Ek/LIC
Expression host	*E. coli* BL21 Rosetta2
Construct sequence	MAHHHHHHVDDDDKMENLYFQ|GDQVKKRKKKRKDYQP-NYFLSIPITNKEIIKGIKILQNAIIQQDERLAKAMV-SDGSFHITLLVMQLLNEDEVNIGIDALLELKPFIEE-LLQGKHLTLPFQGIGTFGNQVGFVKLAEGDHVNSLL-EIAETANRTFQEKGILVGESRSFKPHLTFMKLSKSP-WLRKNGVKKIDPDLYEKFISHRFGEEILYRIDLCSM-LKKKQSNGYYHCESSIVIGEK

Table 2
Crystallization.

Method	Sitting drop
Plate type	24-well Cryschem plate (Hampton Research)
Temperature (K)	291
Protein concentration (mg ml^{-1})	20
Buffer composition of protein solution	500 m*M* NaCl, 5 m*M* Tris–HCl pH 8.0, 1 m*M* DTT
Composition of reservoir solution	2.5 *M* sodium malonate pH 7.0
Volume and ratio of drop	1:1, 2 µl total
Volume of reservoir (µl)	250

(Ni–NTA column, GE Healthcare) in equilibration buffer (500 m*M* NaCl, 20 m*M* Tris–HCl pH 8.0, 40 m*M* imidazole, 5 m*M* β-mercaptoethanol) using an ÄKTAprime FPLC system. The column was washed with ten column volumes (CV) of equilibration buffer and the 6×His-tagged protein was released with elution buffer (500 m*M* NaCl, 20 m*M* Tris–HCl pH 8.0, 300 m*M* imidazole, 5 m*M* β-mercaptoethanol). The peak fractions were collected and evaluated by SDS–PAGE. GFP/His-tagged TEV protease was added in a 1:50 ratio and dialyzed overnight against dialysis buffer (500 m*M* NaCl, 15 m*M* Tris–HCl pH 8.0, 5 m*M* β-mercaptoethanol, 40 m*M* imidazole). The digested protein was again loaded onto a pre-equilibrated Ni^{2+}-affinity column and the flow-through fraction containing the untagged hAKAP18γ^{CD} was collected. The protein was concentrated (10 kDa MWCO Vivaspin filter, GE Healthcare) and the concentrated sample was loaded onto a Superdex 200 HiLoad 10/600 prep-grade column as a final purification step using an ÄKTApurifier HPLC system. UV absorption was recorded at 280 nm. Fractions containing the purified protein were collected and its purity was determined by SDS–PAGE. SDS–PAGE analysis of various steps of purification and a size-exclusion chromatogram are shown in Fig. 1. Macromolecule-production information is given in Table 1.

2.2. Crystallization

Purified hAKAP18γ^{CD} was concentrated to 20 mg ml^{-1}, including a shift in the buffer conditions to 500 m*M* NaCl, 5 m*M* Tris–HCl pH 8.0, 1 m*M* DTT, using a 10 kDa MWCO Vivaspin column (GE Healthcare) in an Allegra X-22R centrifuge (Beckmann Coulter) at 3000*g* at 4°C. Concentration was measured with a NanoDrop 2000 (Thermo Scientific) using a predicted extinction coefficient of 14 440 M^{-1} cm^{-1}. Crystallization was performed by vapour diffusion in a sitting-drop setup in a 24-well plate (Hampton Research) in accordance with Table 2. The plate was sealed with Crystal Clear tape (Hampton Research) and placed at 18°C. Crystals appeared within 5 d. Single crystals were mounted using a LithoLoop (Molecular Dimensions) of suitable size, flash-cooled directly from the drops without the need for additional cryoprotectant and stored in liquid nitrogen at 100 K.

Table 3
Data collection and processing.

Values in parentheses are for the outer shell.

Diffraction source	ID30B, ESRF
Wavelength (Å)	0.976
Temperature (K)	100
Detector	Pilatus 6M
Crystal-to-detector distance (mm)	190.0
Rotation range per image (°)	0.05
Total rotation range (°)	360
Exposure time per image (s)	0.037
Space group	$P2_12_12_1$
a, *b*, *c* (Å)	56.3, 60.3, 65.5
Mosaicity (°)	0.2
Resolution range (Å)	44.4–1.25
Total No. of reflections	753246 (48408)
No. of unique reflections	119131 (8220)
Completeness (%)	99.8 (98.9)
Multiplicity	6.3 (5.5)
$\langle I/\sigma(I)\rangle$†	18.49 (1.49)
$CC_{1/2}$ (%)	99.9 (54.0)
R_{meas} (%)	0.047 (1.166)
Overall *B* factor from Wilson plot (Å^2)	22.76

† Mean $I/\sigma(I)$ falls below 2.0 at 1.28 Å resolution. The data were cut with the aim of a $CC_{1/2}$ value of 50%.

2.3. Data collection and processing

Diffraction data collection was carried out on beamline ID30B at the European Synchrotron Radiation Facility (ESRF), Grenoble, France. The beamline features a Dectris Pilatus 6M detector. The crystal lattice was determined to be primitive orthorhombic and a data-collection strategy was performed in *iMosflm* (Battye *et al.*, 2011). A data set was collected at 1.25 Å resolution. Data reduction was performed using *xia*2 (Winter *et al.*, 2013) in space group $P2_12_12_1$. Data-collection and processing statistics are collected in Table 3.

2.4. Structure solution and refinement

The Matthews coefficient of 2.3 Å^3 Da^{-1} indicated the presence of one molecule in the asymmetric unit with a solvent content of 47% (Kantardjieff & Rupp, 2003). The data were phased using the apo form of rat AKAP18γ (rAKAP18γ; PDB entry 2vfy; Gold *et al.*, 2008) as a search model. rAKAP18γ shares 83% sequence identity with hAKAP18γ^{CD}. The initial model was built using *phenix.autobuild* (Adams *et al.*, 2010) and *Coot* (Emsley & Cowtan, 2004). Model refine-

ment was performed in *phenix.refine* (Adams *et al.*, 2010). Refinement statistics are collected in Table 4. The final model and structure factors have been deposited in the Protein Data Bank with accession code 5jj2.

3. Results and discussion

3.1. The structure of human AKAP18γ^{CD}

The crystal structure of human AKAP18γ^{CD} (hAKAP18γ^{CD}) was refined to a final R_{cryst} and R_{free} of 0.161 and 0.180, respectively. Validation using *MolProbity* (Chen *et al.*, 2010) showed that 99.1% of the residues are located in Ramachandran favoured regions. The structure features a central crevice flanked by two antiparallel β-sheets composed of strands $\beta1$–$\beta2$–$\beta5$–$\beta8$–$\beta9$ and $\beta3$–$\beta4$–$\beta6$–$\beta7$, respectively. These sheets are flanked by α-helices on the side facing away from the crevice (Fig. 2*a*). hAKAP18γ^{CD} is locked in an apo state with no AMP present in the binding pocket; rather, a malonate molecule (M1) occupies this binding crevice. In addition, five additional malonate molecules (M2–M6) were identified; however, their positions appear to be less defined in the electron density. Furthermore, they are not located in the immediate proximity of the R-loop. Their locations on the surface of hAKAP18γ^{CD} are presented in Supplementary Fig. S1.

Table 4
Structure solution and refinement.

Values in parentheses are for the outer shell.

Resolution range (Å)	1.25
No. of reflections, working set	118887
No. of reflections, test set	5820
Final R_{cryst}	0.161
Final R_{free}	0.180
No. of non-H atoms	
Protein	1822
Ligand	56
Water	256
Total	2134
R.m.s. deviations	
Bonds (Å)	0.005
Angles (°)	0.850
Average *B* factors (Å^2)	
Protein	26.5
Ligand	68.7
Water	35.9
Ramachandran plot	
Most favoured (%)	99.1
Allowed (%)	0.9

3.2. Comparison of human AKAP18γ^{CD} with rat AKAP18δ^{CD}

Superposition of the rat and human structures show that the overall fold of hAKAP18γ^{CD} is equivalent to the structure of apo rAKAP18δ^{CD}, with an overall r.m.s.d. value of 0.81 Å

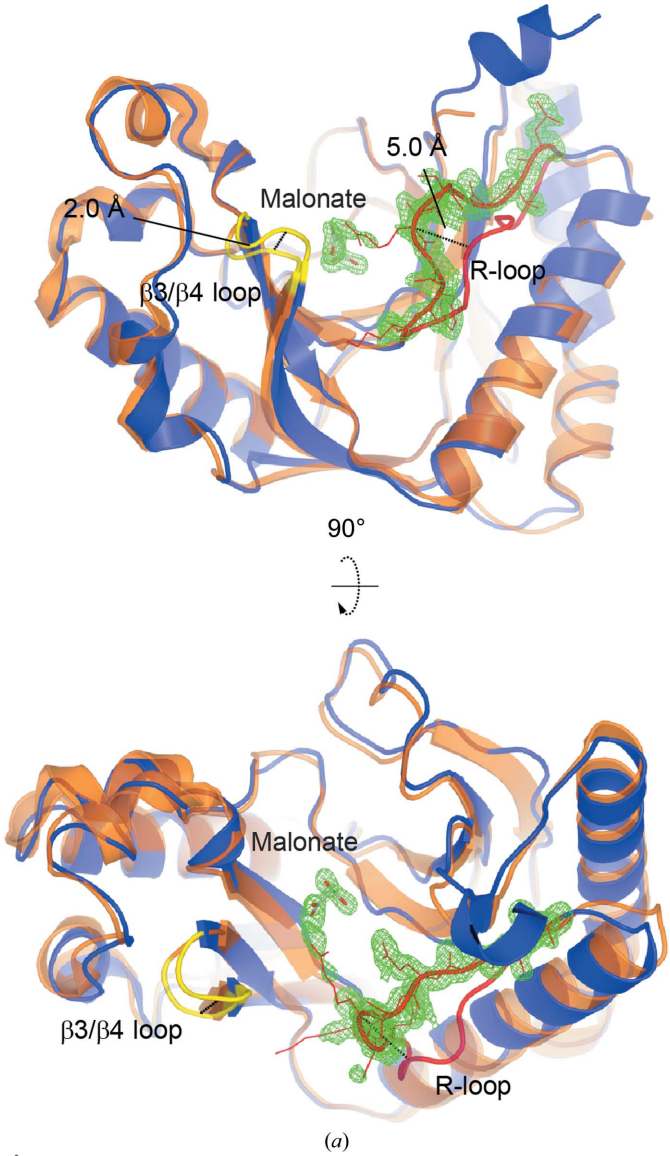

(*a*)

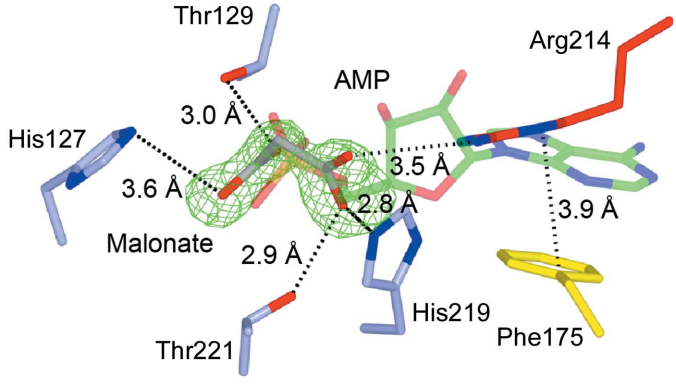

(*b*)

Figure 2
Structure of hAKAP18γ^{CD} (blue) in complex with malonate superposed with the apo structure of rAKAP18δ^{CD} (orange). (*a*) Malonate is found buried in the central crevice of hAKAP18γ^{CD} in close proximity to the R-loop (red) and the $\beta3$/$\beta4$ loop (yellow). The relative displacements of the loop regions are shown. Difference density ($F_o - F_c$) from an OMIT map is shown at 3.5σ for malonate. Difference density for the R-loop is shown at 2.5σ. (*b*) The malonate-binding site superposed with AMP from the structure of rAKAP18δ^{CD}. Malonate binds in the site occupied by the phosphate group of AMP and effectively bridges the residues of the 2H phosphoesterase motif (His127, Thr129, His219 and Thr221) with the R-loop (Arg214). Arg214 forms a π–π interaction with Phe174 in the $\beta3$/$\beta4$ loop.

(Fig. 2*a*). The only differences include the displacement of a highly conserved loop region, termed the R-loop, found between β-sheet $\beta5$ and α-helix $\alpha3$, and a minor displacement of the $\beta3/\beta4$ loop. The relative displacement in the R-loop is 5.0 Å (hAKAP18γ^{CD} Arg214 C^{α} to rAKAP18δ^{CD} Arg214 C^{α}). A difference density ($F_o - F_c$) OMIT map covering the R-loop is included in Fig. 2(*a*) and indicates the new position. In the structures of AMP-bound and CMP-bound rat AKAP18δ^{CD} (PDB entries 2vfk and 2vfl; Gold *et al.*, 2008), the conserved residues Arg214 and Phe174 of hAKAP18γ^{CD} form stacking interactions with the aromatic adenine and cytosine moieties. The majority of the side chain of Arg214 could not be traced in the electron density of rAKAP18δ^{CD}, and only backbone and C^{β} atoms are modelled. However, in the apo form of hAKAP18γ^{CD} the side chain of Arg214 forms a π–π stacking interaction with the phenyl ring of Phe174. The distance between Arg214 N^{ε} and Phe174 C^{γ} was measured to 3.9 Å. Furthermore, this interaction places the positively charged guanidinium moiety of Arg214 in the proximity of a negatively charged malonate molecule found in the crevice. At pH 7.0 and with a distance between the guanidinium and the carboxylate of the malonate of 3.5 Å, an electrostatic interaction is present (Fig. 2*b*). The malonate molecule is further anchored by hydrogen bonding to the side-chain hydroxyl of Thr29, His219 and Thr221. The stacking interaction and local stabilization provided by the malonate are the likely cause of the overall conformational change of the loop.

3.3. The malonate complex resembles the AMP-bound form of human AKAP18γCD

Superposition of the AMP-bound form of rAKAP18δ^{CD} reveals that the guanidinium moiety and the malonate molecule occupy equivalent positions to N9 of the adenine moiety and the phosphate group, respectively (Fig. 2*b*). Attempts have been made to obtain a crystal structure of the AMP-bound form of hAKAP18γ^{CD}; however, under the present crystallization conditions AMP may have been displaced by the high concentration of malonate. Since there is a report of AKAP18 complexes that lack AMP and GMP in the central crevice (Ezerski, 2011), it is possible that both nucleotide adducts are opportunistic interactors rather than physiological ligands. Nonetheless, the prevailing view is that hAKAP18γ^{CD} acts as a low-affinity AMP sensor *in vivo* and it is possible that the AMP-bound form can be mimicked by the presence of malonate to some extent.

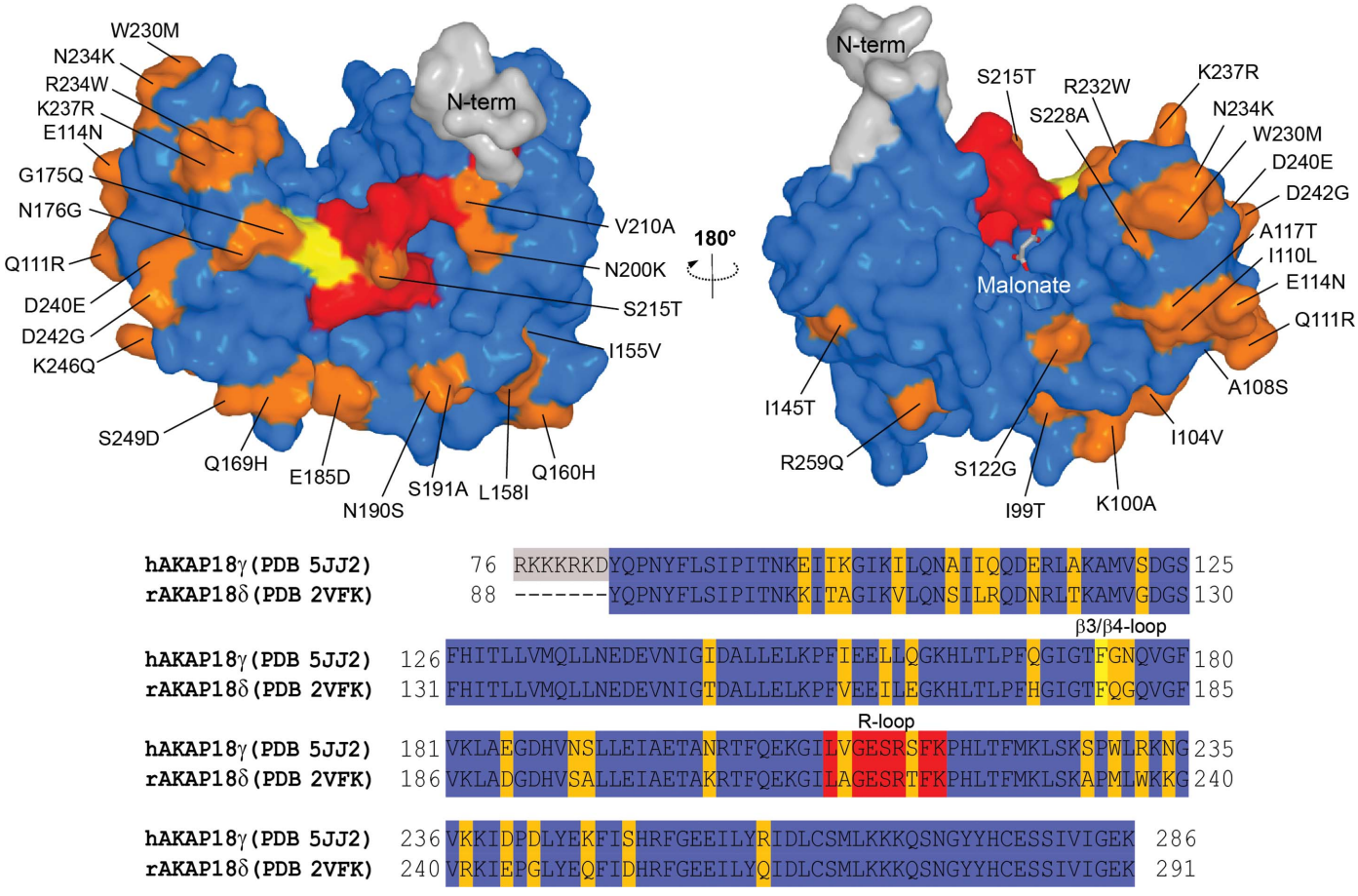

Figure 3
Mapping of amino-acid differences between hAKAP18γ^{CD} and rAKAP18δ^{CD}. Differences are highlighted in orange. R-loop and $\beta3/\beta4$-loop residues are highlighted in red and yellow, respectively.

3.4. Malonate ligands as input for fragment-based drug screening

It is likely that competition with AMP binding will have functional implications for the biology of hAKAP18γ. Hence, the malonate molecule can be used as a starting point for fragment-based drug discovery. The dimensions and charge distribution of malonate seem to be ideal to bridge the aromatic recognition motif (Arg214 and Phe174) with the 2H phosphoesterase motif. From structural alignment of hAKAP18γ^{CD} and rAKAP18δ^{CD}, it is found that sequence variation is found primarily on the surface of the protein and that the residues lining the central crevice are completely conserved (Fig. 3). In addition, the deviating residues appear to cluster at one end of hAKAP18γ^{CD}. This may indicate an as yet unappreciated function for these conserved surfaces. Consequently, inhibitors developed against the nucleotide-binding site may first aid in elucidating the physiological role of AKAP18 and subsequently have significant therapeutic potential.

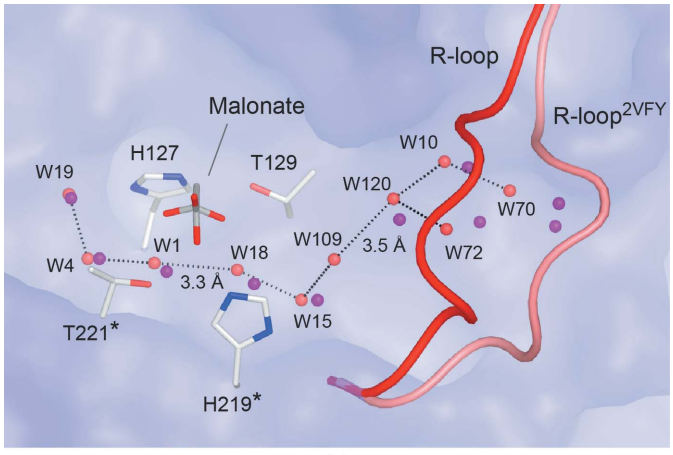

(*a*)

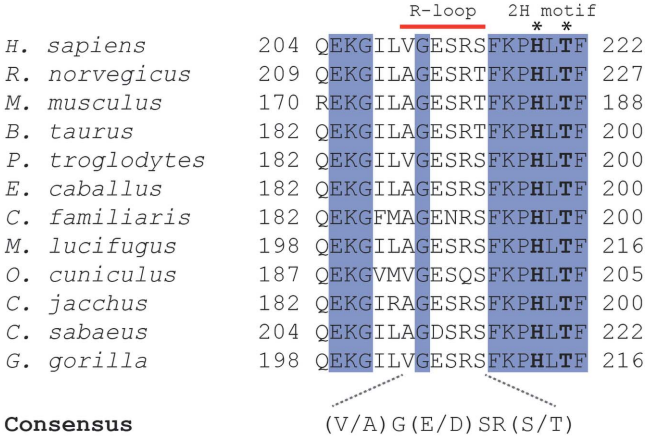

(*b*)

Figure 4
Water structure in the nucleotide-binding crevice and conservation of the R-loop. (*a*) Waters (red) line the bottom of the crevice, forming a hydrated path leading from the 2H phosphodiesterase motif to bulk solvent through the R-loop (red). Water–water distances that are longer than normal hydrogen bonds are labelled. The water structure of hAKAP18γ^{CD} and rAKAP18δ^{CD} (red and purple) is highly conserved around the active site, whereas the dislocation of the R-loop affects the local water structure beneath the loop. (*b*) The R-loop is functionally conserved with the consensus motif (V/A)G(E/D)SR(S/T). Completely conserved residues of the regions flanking the R-loop are marked in blue. These are involved in maintaining the fold of the 2H phosphodiesterase motif. The R-loop is marked with a red bar.

3.5. The active site of hAKAP18γCD contains a putative proton wire

The presence of the 2H phosphoesterase motif formed by Thr127, His129, His219 and Thr221 indicates that hAKAP18γ^{CD} has enzymatic activity; however, its physiological substrate remains unknown. Earlier studies noted a structural similarity to the active site of 2′,3′-cyclic nucleotide 3′-phosphoesterase (CNPase; Myllykoski *et al.*, 2012). One feature shared between CNPase and hAKAP18γ^{CD} is the hydrated substrate-binding crevice. The water found in the binding crevice of hAKAP18γ^{CD} links directly to bulk solvent through the R-loop (Fig. 4*a*). Studies of the catalytic mechanism of CNPase describe the activation of a water molecule prior to nucleophilic attack on the substrate (Myllykoski *et al.*, 2013). This activation requires the abstraction of a proton from the catalytic site, and it is possible that water plays a role in its efficient removal through a proton wire formed by the chain of water molecules. The positions of waters W19, W4, W1 and W18 and W15 are relatively conserved between rAKAP18δ^{CD} and hAKAP18γ^{CD}. The water positions below the R-loop (W109, W120, W10, W70 and W72) are not conserved, which is likely to reflect the variability in the position of the loop and the rearrangement of the local water structure. All distances between water molecules are compatible with hydrogen bonding except for the distances W3–W4 (3.3 Å) and W6–W7 (3.5 Å). One may hypothesize that the correct substrate may arrange the water molecules in this region in a way that may complete the proton wire. This may also explain not only why Arg214 is conserved in the loop, but that the entire loop is composed of a consensus motif (V/A)G(E/D)SR(S/T), which is either completely conserved or with functionally conserved residues, as shown by the alignment (Fig. 4*b*).

In summary, we have determined the crystal structure of the central domain of human AKAP18γ at 1.25 Å resolution. The structure reveals a similar fold to that previously determined from rat AKAP18δ. However, the R-loop region carrying the important residue Arg214, which is involved in interaction with AMP, has moved to a position stabilized by the binding of malonate. The local water structure below the R-loop is rearranged depending on the position of the loop and may be of catalytic importance. The interaction between Phe174 and Arg214 combined with the position of the malonate molecule in stabilization leads to the suggestion that this state of hAKAP18γ^{CD} resembles the AMP-bound form to some extent. This observation may be of further use in investigation of the role of hAKAP18 in AMP sensing and in drug screening.

Acknowledgements

The authors would like to thank the ESRF and beamline staff for the beam time and support during data collection at ID30B. This work has been funded by grants from the Lundbeck Foundation (KBA), the University of Oslo (EØ) and the Norwegian Research Council (KT and JPM). JDS is an investigator of the Howard Hughes Medical Institute and is supported in part by NIH grants DK054441 and DK105542.

References

Adams, P. D. *et al.* (2010). *Acta Cryst.* D**66**, 213–221.
Battye, T. G. G., Kontogiannis, L., Johnson, O., Powell, H. R. & Leslie, A. G. W. (2011). *Acta Cryst.* D**67**, 271–281.
Beene, D. L. & Scott, J. D. (2007). *Curr. Opin. Cell Biol.* **19**, 192–198.
Carr, D. W., Stofko-Hahn, R. E., Fraser, I. D., Bishop, S. M., Acott, T. S., Brennan, R. G. & Scott, J. D. (1991). *J. Biol. Chem.* **266**, 14188–14192.
Chen, V. B., Arendall, W. B., Headd, J. J., Keedy, D. A., Immormino, R. M., Kapral, G. J., Murray, L. W., Richardson, J. S. & Richardson, D. C. (2010). *Acta Cryst.* D**66**, 12–21.
Emsley, P. & Cowtan, K. (2004). *Acta Cryst.* D**60**, 2126–2132.
Ezerski, V. E. (2011). Dissertation. Freie Universität Berlin, Germany.
Gold, M. G., Smith, F. D., Scott, J. D. & Barford, D. (2008). *J. Mol. Biol.* **375**, 1329–1343.
Kantardjieff, K. A. & Rupp, B. (2003). *Protein Sci.* **12**, 1865–1871.
Langeberg, L. K. & Scott, J. D. (2015). *Nature Rev. Mol. Cell Biol.* **16**, 232–244.
Lygren, B., Carlson, C. R., Santamaria, K., Lissandron, V., McSorley, T., Litzenberg, J., Lorenz, D., Wiesner, B., Rosenthal, W., Zaccolo, M., Taskén, K. & Klussmann, E. (2007). *EMBO Rep.* **8**, 1061–1067.
Myllykoski, M., Raasakka, A., Han, H. & Kursula, P. (2012). *PLoS One*, **7**, e32336.
Myllykoski, M., Raasakka, A., Lehtimäki, M., Han, H., Kursula, I. & Kursula, P. (2013). *J. Mol. Biol.* **425**, 4307–4322.
Smith, F. D., Reichow, S. L., Esseltine, J. L., Shi, D., Langeberg, L. K., Scott, J. D. & Gonen, T. (2013). *Elife*, **2**, e01319.
Taskén, K. & Aandahl, E. M. (2004). *Physiol. Rev.* **84**, 137–167.
Winter, G., Lobley, C. M. C. & Prince, S. M. (2013). *Acta Cryst.* D**69**, 1260–1273.
Wong, W. & Scott, J. D. (2004). *Nature Rev. Mol. Cell Biol.* **5**, 959–970.
Zaccolo, M. & Pozzan, T. (2002). *Science*, **295**, 1711–1715.